Hindawi
Geofluids
Volume 2022, Article ID 2948701, 13 pages
https://doi.org/10.1155/2022/2948701

Research Article

Apatite Fission Track Thermochronology of Granite from Duobaoshan Porphyry Cu (Mo) Deposit, Northeast China: Implications for Cooling History and Ore Preservation

Yaxing Leng,[1,2] **Jianping Wang**,[2] **and Dewen Zheng**[3]

[1]*Chinese Academy of Geological Sciences, Beijing 100037, China*
[2]*China University of Geosciences (Beijing), Beijing 100083, China*
[3]*Guangzhou Institute of Geochemistry, Chinese Academy of Sciences, Guangzhou 510640, China*

Correspondence should be addressed to Yaxing Leng; yaxing.leng@gmail.com

Received 10 January 2022; Accepted 19 February 2022; Published 8 March 2022

Academic Editor: Dongdong Ma

The Duobaoshan Cu (Mo) deposit is one of the oldest super large porphyry deposits in the eastern part of the Central Asian orogenic belt. Although ore-forming processes have been extensively concerned, the post-mineralization ore preservation state was poorly focused on. In order to improve the ability of prospecting forecast, it is necessary to consider both deposit formation and deposit preservation. Here, we reported apatite fission track (AFT) data for the Duobaoshan porphyry copper deposits in the belt to reveal the cooling and exhumation history and evaluate ore preservation. The results show that the rapid cooling of the ore-hosting rock body occurred later than the surrounding rock body. The rapid cooling of the surrounding granodiorite occurred between 82 and 72 Ma, with the exhumation depth of 2.33–3.11 km and the exhumation rate of 0.25 mm/a, whereas the ore-hosting granodiorite porphyry was rapid cooling between 71.8 and 50.2 Ma, with the exhumation depth of 2.99–3.86 km and the exhumation rate of 0.22 mm/a. This differential exhumation and cooling event provide favorable geological conditions for the preservation of the ore body.

1. Introduction

Porphyry Cu (Mo) deposits are distributed in rocks formed in different periods from the Archean to the present, but mainly formed in the Meso–Cenozoic, and are spatially concentrated in three tectonic metallogenic regions: the Pacific belt, the Tethys region and the Central Asian–Mongolian–Hinggan region. More than half of the 25 largest known porphyry copper deposits, formed during three periods: the Paleocene–Eocene, Eocene–Oligocene, and middle Miocene–Pliocene [1]. The Miocene porphyry copper deposits such as the Zhunuo deposit in the Gangdese belt of southern Tibet, the post-mineralization granite porphyry yielded a zircon U-Pb age of 12.0 ± 0.2 Ma and molybdenite Re-Os isotopic data indicate mineralization likely occurred from 14.8 ± 0.1 Ma to 13.5 ± 0.1 Ma [2]. The formation depth of porphyry deposits is generally 1–6 km, though some were emplaced deeper [3, 4]. Therefore, most porphyry deposits formed before the Mesozoic have been destroyed or even exhumated completely.

The porphyry Cu (Mo) deposits that formed before the Mesozoic are mainly located in the Central Asian–Mongolian–Hinggan Paleozoic Orogenic Belt, and the Duobaoshan porphyry Cu (Mo) deposit is one such deposit. According to Liu et al. [5], the sulfide Re-Os isochronal age of one molybdenite sample from the Duobaoshan Cu (Mo) deposit was 485.6 ± 3.7 Ma, and the model ages of five chalcopyrite and two pyrite samples were 485.8 ± 2.7 and 481.9 ± 6.7 Ma, respectively. Thus, the mineralization age is consistent with the age of the early Paleozoic granitoids include a biotite granodiorite with a zircon SHRIMP U-Pb age of 479.5 ± 4.6 Ma and a granite porphyry [6, 7]. The mineralization age of the Duobaoshan deposit is between 482 and 486 Ma, and mantle fluid and materials were involved in the mineralization process. The Duobaoshan deposit is a classic porphyry Cu (Mo) deposit that formed in an early

Paleeozoic island arc tectonic setting [5]. The Central Asian orogenic belt has this important feature that the Early Paleozoic porphyry deposits have been preserved, which is different from the Tethys and Circum-Pacific belts. Then, taking the Duobaoshan porphyry Cu (Mo) deposit in the Central Asian orogenic belt as an example to analyze the preservation process of some Early Paleozoic porphyry deposits should be of great significance and also have a certain indication for prospecting and exploration.

The Duobaoshan Cu (Mo) deposit is one of the most important super-large porphyry copper deposits in the northeast China. A variety of former studies have focused on the metallogenic model [8, 9] and geochemical characteristics of the ore deposit [10, 11], the diagenetic and metallogenic age [12, 13], characteristics of the metallogenic fluids [5, 14], and metallogenic regularities [15–17]. However, no study has previously focused specifically on the post-ore change and preservation of this ancient porphyry deposit. In this study, the fission track (FT) and thermal structural analysis were adopted to conduct chronological research on the ore-hosting granodiorite porphyry to determine the timing and rates of cooling and exhumation in the Meso–Cenozoic period, and to constrain the preservation process of the Duobaoshan porphyry Cu deposit.

2. Geological Setting

The Duobaoshan porphyry Cu (Mo) deposit, located in the northwestern part of the, is one of the largest Cu (Mo) deposits in the Central Asian orogenic belt [7, 18–21]. Northeast China consists of the Erguna, Xing'an, Songnen and Jiamusi blocks along the Tayuan–Xiguitu, Nenjiang and Mudanjiang faults, respectively (Figure 1(a)). The Erguna block was tectonically stable before the collision with the Xing'an block along the Tayuan–Xiguitu fault from the early Paleozoic period [22, 23]. The Songnen block joined the composite block along the Nenjiang fault during the late Paleozoic period [22]. The Jiamusi block accreted to this merged block along the Mudanjiang fault during the Mesozoic period (~219 Ma) [22]. The Duobaoshan porphyry Cu (Mo) deposit is located in the Xing'an block (Figure 1(a)).

The lithostratigraphic units in the Duobaoshan area are mainly Ordovician and Silurian, with small areas of Devonian and Cretaceous strata (Figure 1(b)). The Ordovician strata include the Tongshan and Duobaoshan formations, which are composed of terrigenous clastic rocks and intermediate-acid volcanic-volcanoclastic rocks, respectively [18, 20]. The Duobaoshan Formation, with a high Cu abundance, has been considered to be the local source bed of Cu mineralization [9, 24]. The Silurian strata consist of terrestrial clastic rocks and intermediate-basic volcanic rocks. The Devonian strata are composed of sandstone, silty sandstone, argillaceous slate, andesite, dacite, tuff lava and spilite with lenses of limestone. The Cretaceous strata are terrestrial and coal-bearing.

The Duobaoshan ore district has undergone at least three magmatic events, the Ordovician period (470–480 Ma), Triassic period (230–240 Ma), and early Jurassic period (170–180 Ma) [25]. The major magmatic rocks in this district are granodiorite, granodiorite porphyry, and veins of trondhjemite and diorite porphyry that intruded along the NE-trending fissures in the late stage. The Cu mineralization in the Duobaoshan deposit is closely related to the granodiorite porphyry. The Cu ore body is mainly hosted in the granodiorite (Figure 2(a)). It extends along the NW–SE arc structure, and the rock body plunges toward the SW. Intensive alteration of granodiorite can be observed in an open pit, including propylitization at the periphery of the granodiorite and phyllic alteration of the surrounding rock (Figure 2(b)). The contact surface between the rock body and the surrounding rock is mostly in a canine-tooth shape, and a small part of the rock body penetrates into the surrounding rock in the form of small rock dendrites. The surrounding rocks in the contact zone and the trapped bodies in the rock have undergone a certain degree of thermal metamorphism, but the degree is slightly different. Biotization and hornlitification usually develop in the contact zone, and alteration can be seen in local areas. The thermal metamorphism of the surrounding rocks is not only weak but also very uneven. At the same time, the composition of minerals has a clear zonation relationship. There are more quartz-mica diorite facies belts at the edges of the rock body, while granodiorite facies belts can be seen gradually into the interior of the rock body.

Granodiorite and granodiorite porphyry are the major granitoids in the area, although many other kinds of intrusions rocks are also present (Figure 1(b)). The early Palaeozoic granitoids include a biotite granodiorite with a zircon SHRIMP U-Pb age of 485 ± 8 Ma and a granite porphyry [7]. The late Palaeozoic granitoids are mainly granodiorite, granodiorite porphyry, quartz diorite and tonalite with reported whole rock K-Ar isochron ages of 292 Ma for the granodiorite and 283 Ma for the granodiorite porphyry [18]. According to the compiled isotopic ages (K-Ar and Rb-Sr isochron ages) of hornblende, biotite and the whole rock, the granodiorite in the area was likely emplaced two periods, about 226 Ma and 310 Ma, respectively [19]. The Mesozoic granitoids are mainly amphibole granodiorite, biotite granodiorite and minor alkaligranite and fine-grained diorite, yielding zircon SHRIMP U-Pb ages between 176 ± 3 Ma and 177 ± 3 Ma [7]. The Mesozoic granitoids are considered to be related to the Au mineralization in the area [26].

The structure of the Duobaoshan mining area mainly consists of NW-trending structures, NW-trending arc structures and NE-trending structures. The NW-trending structural belt, consisting of a series of folds and faults, is approximately 25 km long and displays a reverse "S" shape [20, 27]. The folds are well developed, mainly comprising the Duobaoshan compound inverted anticline, which includes a closed ring of steep inclined folds, a compound anticline, and accompanying syncline. The main active period of this compound structure likely occurred at the end of the Early Carboniferous period and persisted until the late Permian period. Orebody No. 3 of the Duobaoshan copper deposit in the study area is located at the core of the syncline structure accompanied by the NW-trending compound anticline and syncline. There are at least three NW-

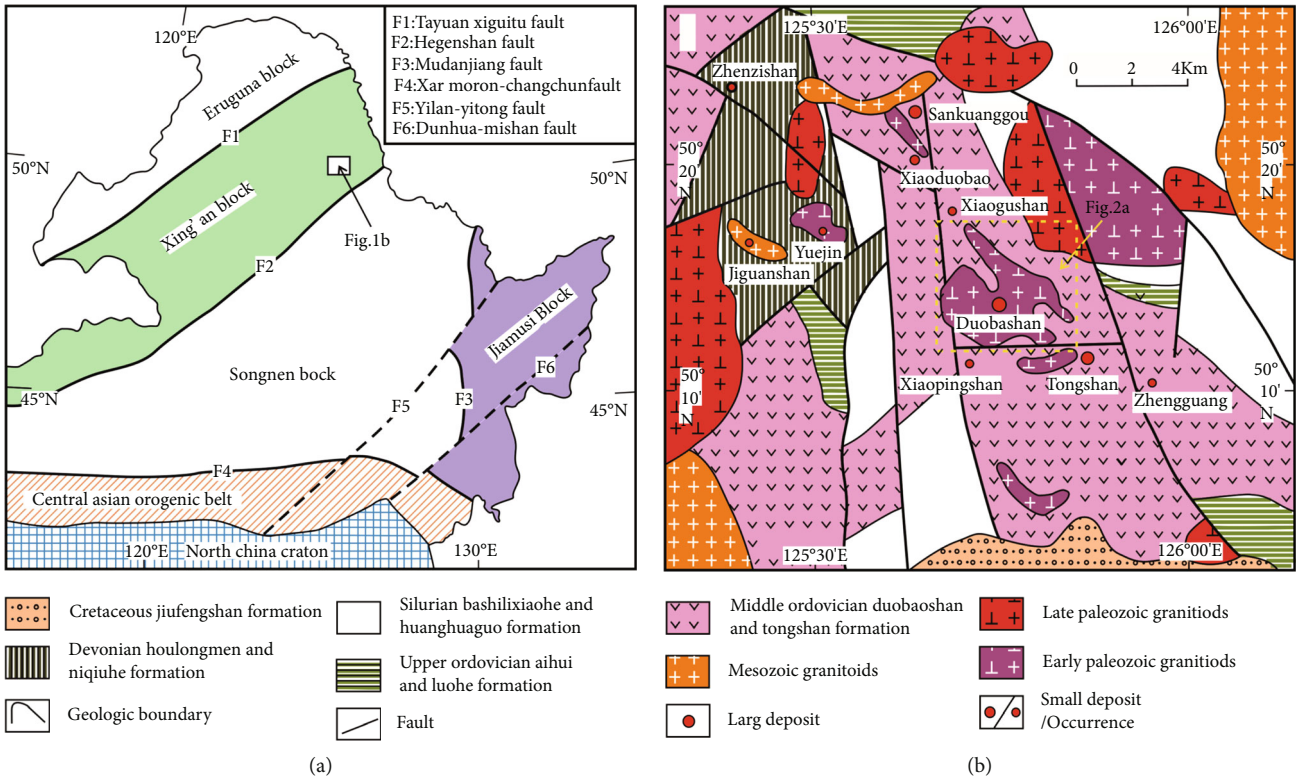

Figure 1: Sketch tectonic map (a) and regional geological map (b) of the Duobaoshan porphyry Cu (Mo) deposit [7, 20].

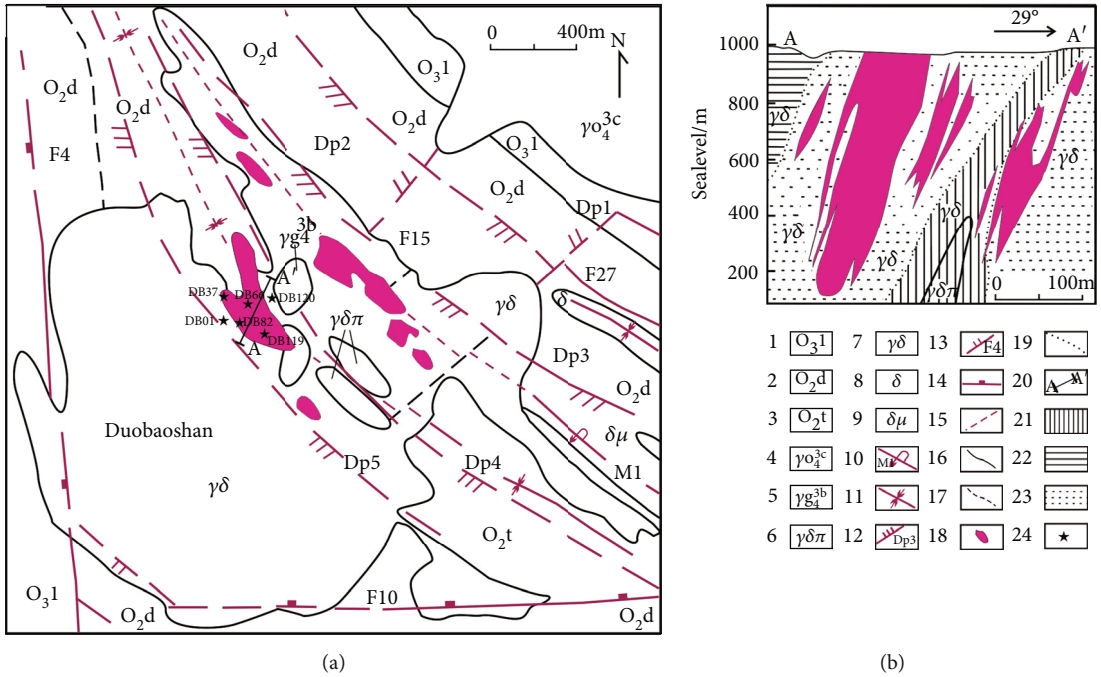

Figure 2: Simplified geological tectonic map (a) and schematic section of ore belt No. 3 (b) of the Duobaoshan porphyry Cu (Mo) deposit [9, 18]. 1-Luohe Formation; 2-Duobaoshan Formation; 3-Tongshan Formation; 4-Plagiogranite; 5-Trondhjemite; 6-Granodiorite porphyry; 7-Granodiorite; 8-Diorite; 9-Diorite porphyrite; 10-The inverted anticline and its serial number; 11-Synclinal axis; 12-Compression-torsional arc fracture fragmentary zone and Number; 13-Fault and Number; 14-Compression-torsional fault; 15-Field measurement and prediction of faults; 16-Observed geologic boundary; 17-Speculated geological boundary; 18-Ore body; 19-Alteration zone boundary; 20-Section line; 21-Potassic alteration zone; 22-Propylitic alteration zone; 23-Phyllic alteration zone; 24-Sampling locations.

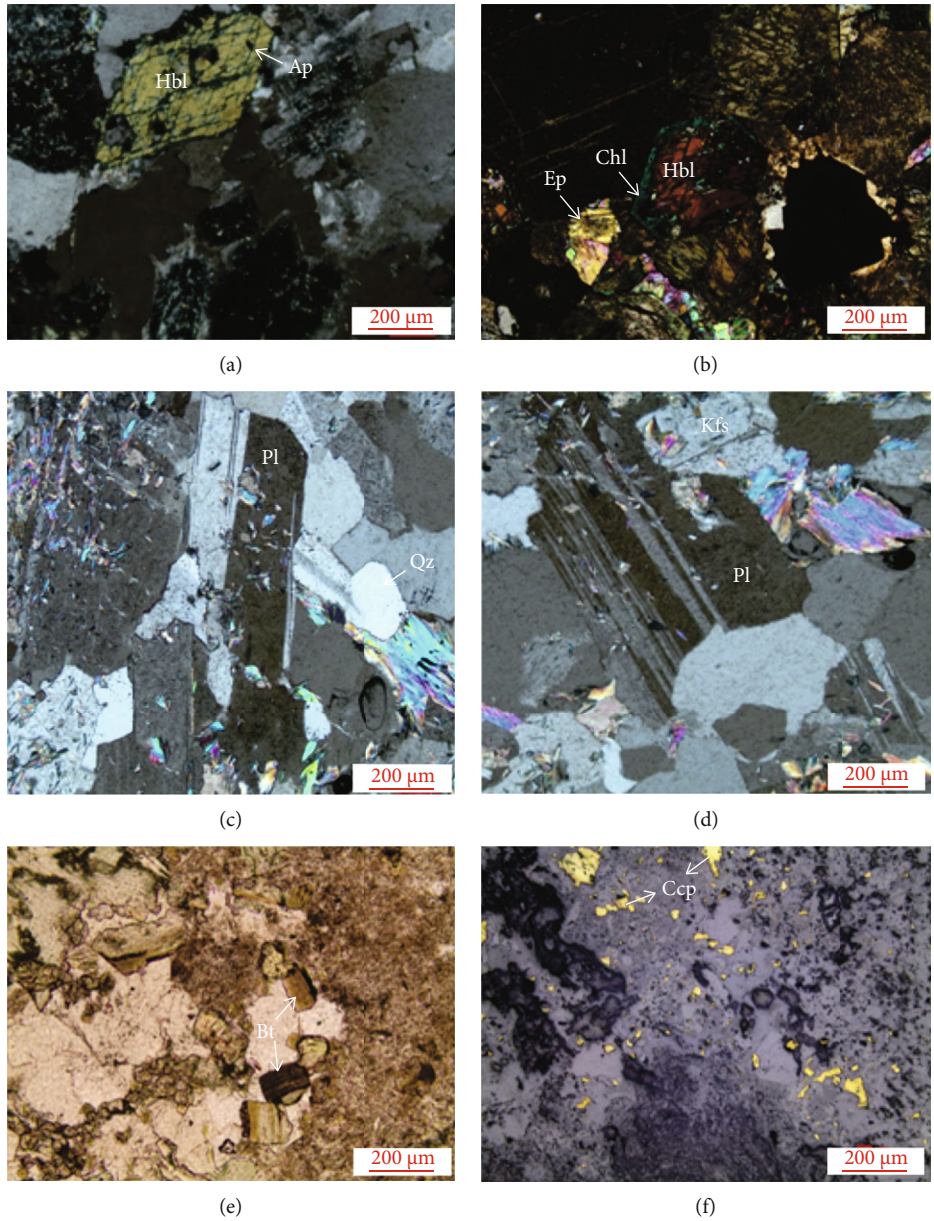

Figure 3: Representative photomicrographs for granites in the Duobaoshan area. Hbl-Hornblende; Ap-apatite; Ep-Epidote; Chl-Chlorite; Qz-Quartz; Pl-Plagioclase; Kfs-K–feldspar; Bt-Biotite; Ccp-Chalcopyrite.

trending compressive and torsional faults in the NW-trending fault structure. They are composed of strong fragmentary fracture zones, which controlled the formation of ore bodies and caused the ore group of Duobaoshan to appear in an en-echelon ramp structure (Figure 2(a)). The NW-trending arcuate structural belt is composed of strata, intrusive rocks, fault zones, schistositized zones, alteration zones and ore zones. The arcuate belt was formed by superimposition and reconstruction based on the NW-trending structural belt. Consequently, several groups of structures intersect in the area, providing channels for metallogenic fluids and space for ore storage, and the ore bodies are mostly located in this structural belt [16]. Therefore, the NW-trending arcuate tectonic belt has laid a favorable tectonic framework for magmatism and mineralization of the Duobaoshan ore field and controlled the formation of ore bodies.

The granodiorite porphyry is medium-grained and consists of plagioclase (55% of the rock body), hornblende (10–20%), quartz (15–20%), and potassium feldspar (5–12%), with minor amounts of biotite (5–8%) (Figures 3(a)–3(f)). The plagioclase is generally automorphic and subhedral crystal and is twinned (Figures 3(c), 3(d)). Accessory minerals include zircon, apatite, titanite, and magnetite. Moreover, most of these samples are slightly sericitized, chloritized, and argillic-altered.

Table 1: Sample description of the Duobaoshan copper deposit.

Sample number	Location	Longitude E	Latitude N	Elevation (m)	Rock type
DB01	Wallrock	125°46′50″	50°14′37″	505	Granodiorite
DB82	Orebody	125°47′02″	50°14′36″	475	Granodiorite porphyry
DB37	Orebody	125°46′51″	50°14′54″	490	Granodiorite porphyry
DB66	Orebody	125°47′08″	50°14′49″	475	Granodiorite porphyry
DB119	Orebody	125°47′20″	50°14′28″	512	Granodiorite porphyry
DB120	Wallrock	125°47′26″	50°14′53″	532	Granodiorite
DB07	Rock vein	125°46′50″	50°14′37″	505	Diorite vein
DB98	Rock vein	125°47′02″	50°14′36″	475	Diorite vein
DB14	Rock vein	125°46′51″	50°14′54″	490	Trondhjemite
DB18	Rock vein	125°47′08″	50°14′49″	475	Trondhjemite
DB99	Rock vein	125°47′20″	50°14′28″	512	Trondhjemite
DB118	Rock body	125°47′26″	50°14′53″	532	Granite porphyry

3. Sample and Analytical Methods

3.1. Sample locations. Samples for apatite fission track (AFT) analysis were collected from the open pit of the Duobaoshan porphyry Cu deposit. Four samples were collected from the ore body (granodiorite porphyry), and two samples were collected from the surrounding granodiorite (Table 1). Others are collected from the late rock body, so this article mainly analyzes the exhumation and cooling history of ore bodies and surrounding rocks. The samples were crushed at the Institute of Regional Geology and Mineral Survey, Hebei Province, China, until the particle size of the minerals in the rocks was suitable, generally about 60 mesh size. After rough separation by traditional methods, apatite was purified by means of electromagnetic separation and heavy liquid separation.

3.2. Analytical methods. Apatite grains were mounted in epoxy resin and polished to expose internal grain surfaces at room temperature. Spontaneous tracks were revealed by etching using 5.5 M HNO_3 for 20 s at 21°C [28]. The weaker etchant and lower temperature resulted in more underetched tracks, leading to shorter mean track lengths. Pressure and stress can also affect the annealing behavior of fission tracks. It is found that continuous supercharging will slow down the annealing rate, and the annealing behavior is even independent of temperature under high stress. Low-uranium muscovite external detectors were packed together with sample grain mounts and Corning CN5 glass dosimeters irradiated in the 492 swimming pool hot-neutron nuclear reactor at the China Institute of Atomic Energy, Beijing. The external detectors were low-umica, and the etching conditions were 40% HF for 40 min at 25°C. FT densities were measured at 1000× magnification under the AUTOSCAN system at the Institute of Geology, China Earthquake Administration. To increase the number of observable horizontal confined tracks, the samples were exposed to ^{252}Cf [29]. The confirmed apatite grains were used to obtain FT data by the external detectors method and the zeta (ξ) calibration method [30]. The anisotropy is calibrated by projecting FT length onto the c-axis using an empirical model [31]. The χ^2 test was used to evaluate the degree of congruence between single apatite ages and all apatite ages in a sample [32, 33]. The grain age distributions were subjected to the χ^2 test to detect whether they contained any extra-Poissonian error. A χ^2 probability≥5% is indicative of a homogeneous population [34].

For samples, track lengths were measured by digitizing the track ends using a drawing tube, and the diameter of etch pit (defined as Dpar) was measured in the dated crystals, to constrain their annealing kinetics [35, 36]. Thermal history modelling for individual samples was carried out using the HeFTy software [37]. AFT data were modelled using c-axis projected lengths and the multi-kinetic annealing model of Ketcham et al. [31], with Dpar as a kinetic parameter. In each of the model simulations, the sample-specific kinetic data (Dpar) were used. Ten thousand t-T paths were randomly generated using a Monte Carlo algorithm.

4. Results and Analysis

The AFT age and track length results are shown in Table 2. The FT age test P (χ^2) of the six samples was greater than 5%, indicating that the single particle ages of the samples belonged to the same group age. A chi-squared probability >5% passed the χ^2 test, and the pooled apatite fission-track age is used for interpretation; a chi-squared probability ≤5% fail the χ^2 test, and the mean apatite fission-track age is used for interpretation. The AFT ages of the six samples range between 50.2 ± 3.0 and 76.0 ± 3.8 Ma. Samples DB01 and DB120 were collected from the surrounding rock and yielded AFT ages of 71.8 ± 3.5 Ma and 76.0 ± 3.8 Ma, respectively. Samples DB37, DB66, DB82 and DB119 were collected from the orebody No. 3 and had AFT ages of 50.2

Table 2: Apatite fission track (AFT) results of samples from the Duobaoshan copper deposit.

Sample number	Nc	$\rho_d(N_d)$ ($\times10^6$ cm^{-2})	$\rho_s(N_s)$ ($\times10^5$ cm^{-2})	$\rho_i(N_i)$ ($\times10^6$ cm^{-2})	U concentration (ppm)	P (χ^2) %	r	Pooled age (Ma $\pm1\sigma$)	Mean track length (μm $\pm1\sigma$)(Nj)	Dpar (μm)	Standard deviation (μm)
DB01	30	0.905 (2261)	5.857 (1233)	1.295(2727)	17.9	57.1	0.936	71.8 ± 3.5	13.76 ± 0.12(100)	1.58	1.28
DB37	30	0.878 (2194)	2.826 (578)	0.869(1777)	12.4	99.6	0.931	50.2 ± 3.0	13.80 ± 0.10(100)	1.60	1.00
DB66	30	0.871 (2178)	2.212 (365)	0.573(945)	8.2	100	0.963	59.1 ± 4.2	13.79 ± 0.11(100)	1.66	1.11
DB82	30	0.864 (2161)	4.178 (988)	1.119(2646)	16.2	86.2	0.890	56.7 ± 2.9	13.82 ± 0.10(100)	1.63	1.02
DB119	30	0.838 (2094)	2.915 (483)	0.808(1338)	12.0	93.2	0.900	53.2 ± 3.4	13.80 ± 0.10(100)	1.72	0.97
DB120	29	0.831 (2077)	5.002 (1189)	0.960(2281)	14.4	64.7	0.899	76.0 ± 3.8	13.67 ± 0.10(100)	1.53	1.07

Notes: Nc = number of apatite crystals analyzed. ρd = induced FT density calculated from muscovite external detectors used with SRM612 dosimeter. Nd = total number of FT counted in ρd. ρs = spontaneous FT density on the internal surfaces of apatite crystals analyzed. Ns = total number of FT counted in ρs. ρi = induced FT density on the muscovite external detector for crystals analyzed. Ni = total number of FT counted in ρi. P (χ^2) = chi-squared probability that all single-crystal ages represent a single population of ages where degrees of freedom = Nc-1 [34]. r = correlation coefficient between Ns and Ni. Nj = number of horizontally confined FT lengths measured. Apatite-Zeta CN5 = 353.0 ±10.

± 3.0 Ma, 59.1 ± 4.2 Ma, 56.7 ± 2.9 Ma and 53.2 ± 3.4 Ma, respectively.

The AFT ages are much younger than the crystallization age of the granodiorite porphyry and the mineralization age. The AFT age represents the age of exhumation cooling, not magmatic cooling. The average fission-track lengths of the samples, its distribution shape and the standard deviation of the length can provide information on the cooling of the samples through the partial annealing zone of the AFTs. If the average fission-track lengths is long, the standard deviation is small. In contrast, if the average fission-track lengths is small, the standard deviation is large and the distribution range of fission-track lengths is wider [38–40]. The average track lengths of all test samples were large and the standard deviations of length were small, ranging from 13.67 to 13.82 μm and 0.97 to 1.28 μm, respectively (Table 2), showing typical characteristics of non-disturbed bedrock [41–43]. The average track lengths of the samples were much smaller than the original track length of 16.3 ± 0.9 μm, as well as smaller than the 14.5–15.5 μm average AFT length associated with rapid cooling to the surface temperature [44]. These results show that the granite was rapidly cooled, and finally was exposed at the surface.

According to the single grain age histogram, sample track length histogram and radial plots, which can visualize the central age, track length distribution peak mode, relative error, tested track number, tested particle number and $P(\chi^2)$ test values (Figure 4), the average track length of the granite samples from the Duobaoshan copper deposit was relatively long, ranging from 13.67 to 13.82 μm, and all values were greater than 12.5 μm, indicating that the samples only experienced one stage of partial annealing in the later period. Their length distribution peaks were all unimodal, barely affected by thermal disturbance in the late stage, and may have remained in the cooling process for the entire time, although this process may have involved both rapid cooling and slow cooling. The track length distribution has a short track tail, meaning that the samples experienced relatively slow cooling through the AFT partial annealing zone; during this period, the FTs experienced a significant annealing shortening effect, and their age does not represent the rapid cooling time of the samples.

5. Thermal Historical Modeling

Apatite fission is a continuous process, and fission track in the minerals records information about a specific stage of the thermal history of the sample below the closure temperature. To obtain further information about the exhumation history of the granite samples from the Duobaoshan copper deposit, a historical thermal model was completed by the program HeFTy [37] following the multi-kinetic annealing model [31]. Monte Carlo simulation was used in modeling operation and took the Dpar values into consideration. Considering that no other low-temperature thermochronological data have been obtained, the con-straints for the AFT thermal modelling in this study include the present-day mean surface temperature of 10 ± 5°C, and the initial temperature of 60 to 200°C (determined by the closure temperatures of AFT). In the simulation process, the initial track length for the temperature calculation was 16.3 μm, and the number of simulation iterations was set at 10,000. To make the exhumation history simulation more reliable, 100 track length measurements and 30 single particle ages were used. Modelling of each sample was finished until obtaining more than 1000 'Acceptable-Fit' paths (merit value: 0.05) and/or more than 20 'Good-Fit' paths (merit value: 0.5).

Six samples at Duobaoshan were obtained successful thermal history modelling results which show one episodes of cooling history characterized by a rapid cooling commencing in the Meso–Cenozoic, a subsequent pronounced residence in the AFT partial annealing zone (Figures 5, 6).

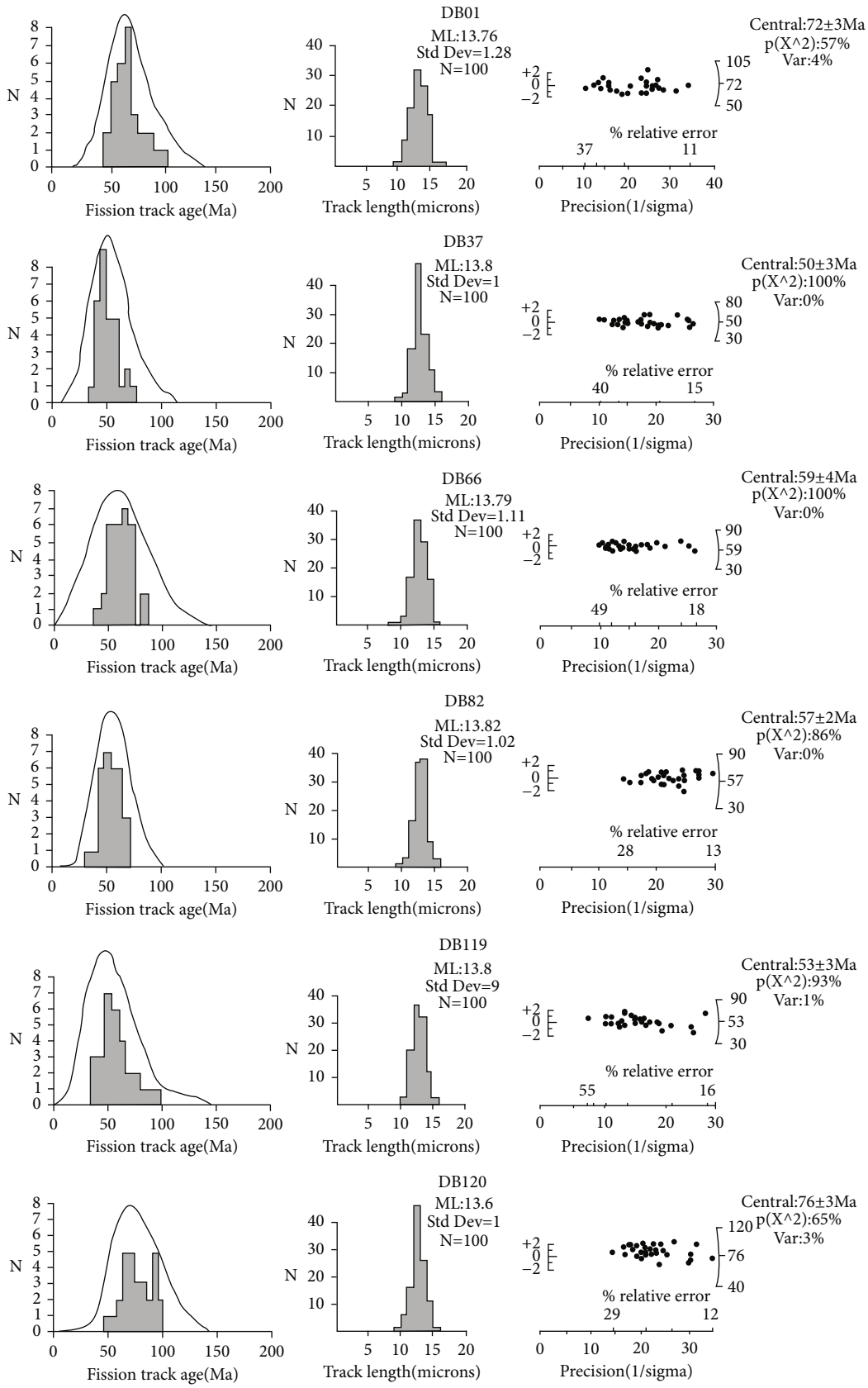

Figure 4: Single grain age histograms, AFT length histograms and radial plots.

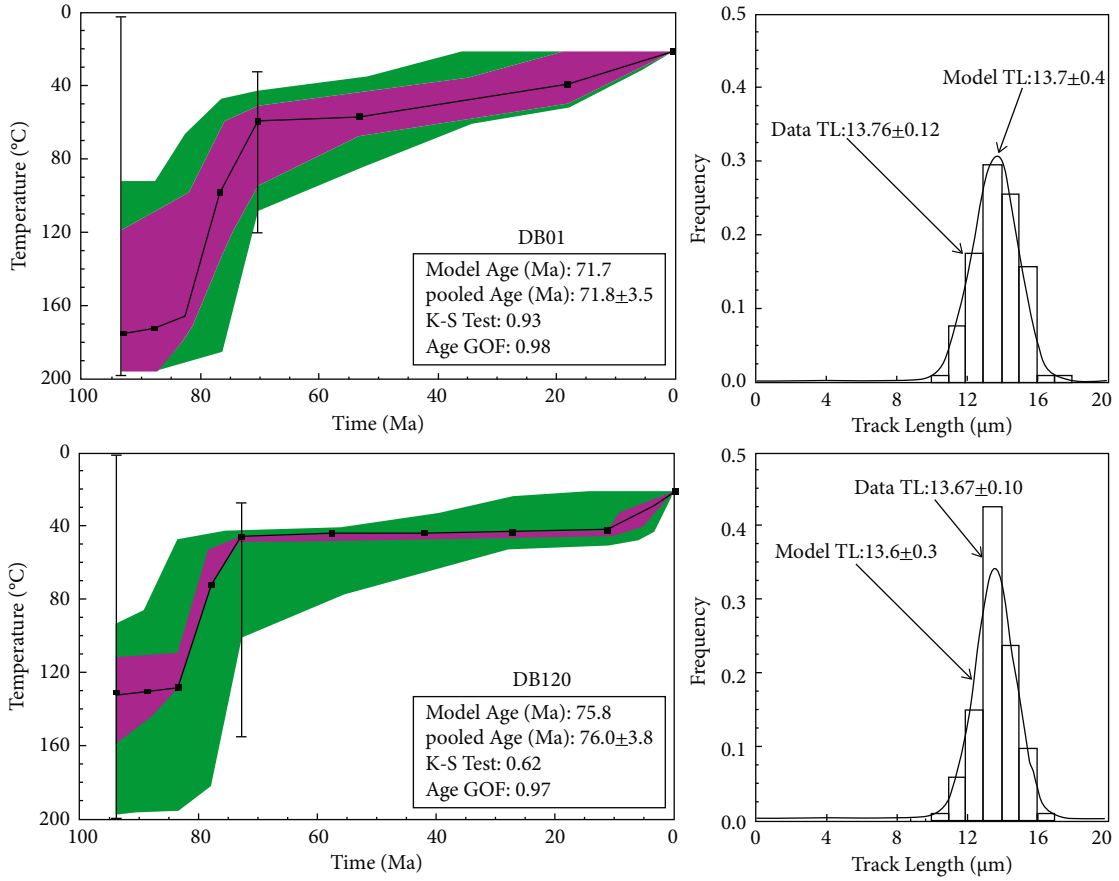

Figure 5: Exhumation history simulation diagram of AFT and histogram of AFT length distribution of the surrounding rocks. The solid line marks the best-fit time-temperature path from which simulated data were derived. Green regions mark envelopes of statistically acceptable fits. Magenta regions indicate envelopes for statistically good fits. I-bars mark user-entered time-temperature constraints.

The "K-S Test" values of all samples were greater than 0.5, except sample DB37 with a value of 0.2. The "Age GOF" values were all greater than 0.5, indicating that the simulation results were highly reliable. Compared with the apparent FT age, the exhumation history simulation results better represent the annealing process of the rock body, provide more intuitive and detailed thermal evolution information, and yield more evidence for the tectonic evolution of the mining area.

6. Discussion

6.1. Meso–Cenozoic cooling and exhumation history at Duobaoshan porphyry copper deposits. The modeling graphs show that the rock body went through rapid and slow exhumation and cooling in the Meso–Cenozoic (Figures 5, 6). The wall rock underwent rapid exhumation and cooling relatively early, during the interval from 82 to 72 Ma. The rapid exhumation and cooling period of the samples from the NW-trending orebody was relatively late, during the interval from 71.8 to 50.2 Ma. After this rapid cooling, a slow cooling period continued until the present. The AFT age and exhumation history simulation results show that the rapid exhumation and cooling of the Duobaoshan granite mainly occurred in the Late Cretaceous.

The AFT system is sensitive to shallow crustal level processes because of the low effective closure temperature, so that, in principle, can be used to trace short-lived variations in the exhumation rate [45]. The AFT closure temperature is 110°C [31, 46, 47]. Assuming a paleo-geothermal gradient of 35°C/km [48] in the research area, which can be used to transfer the cooling rate to the exhumation rate, the results indicate the following: (1) The samples of the surrounding rock body rapidly cooled by 81.7–108.9°C and exhumated by 2.33–3.11 km during the Late Cretaceous to Eocene. The corresponding rapid exhumation period was 10.6–11.5 Ma, and the average exhumation rate was about 0.25 mm/a. (2) The samples of the NW-trending orebody rapidly cooled by 104.7–135.1°C and were exhumated by 2.99–3.86 km. The corresponding rapid exhumation period was 10.6–23.8 Ma, and the average exhumation rate was about 0.22 mm/a. The exhumation rate of the surrounding rocks was larger than that of the orebody, which was favorable for the preservation of the Duobaoshan Cu deposit and consistent with the actual geological conditions.

6.2. Implications for ore preservation and prospecting at Duobaoshan porphyry copper deposits. Based on analysis of the AFT age and exhumation history simulation results, there were three main stages of exhumation and cooling of

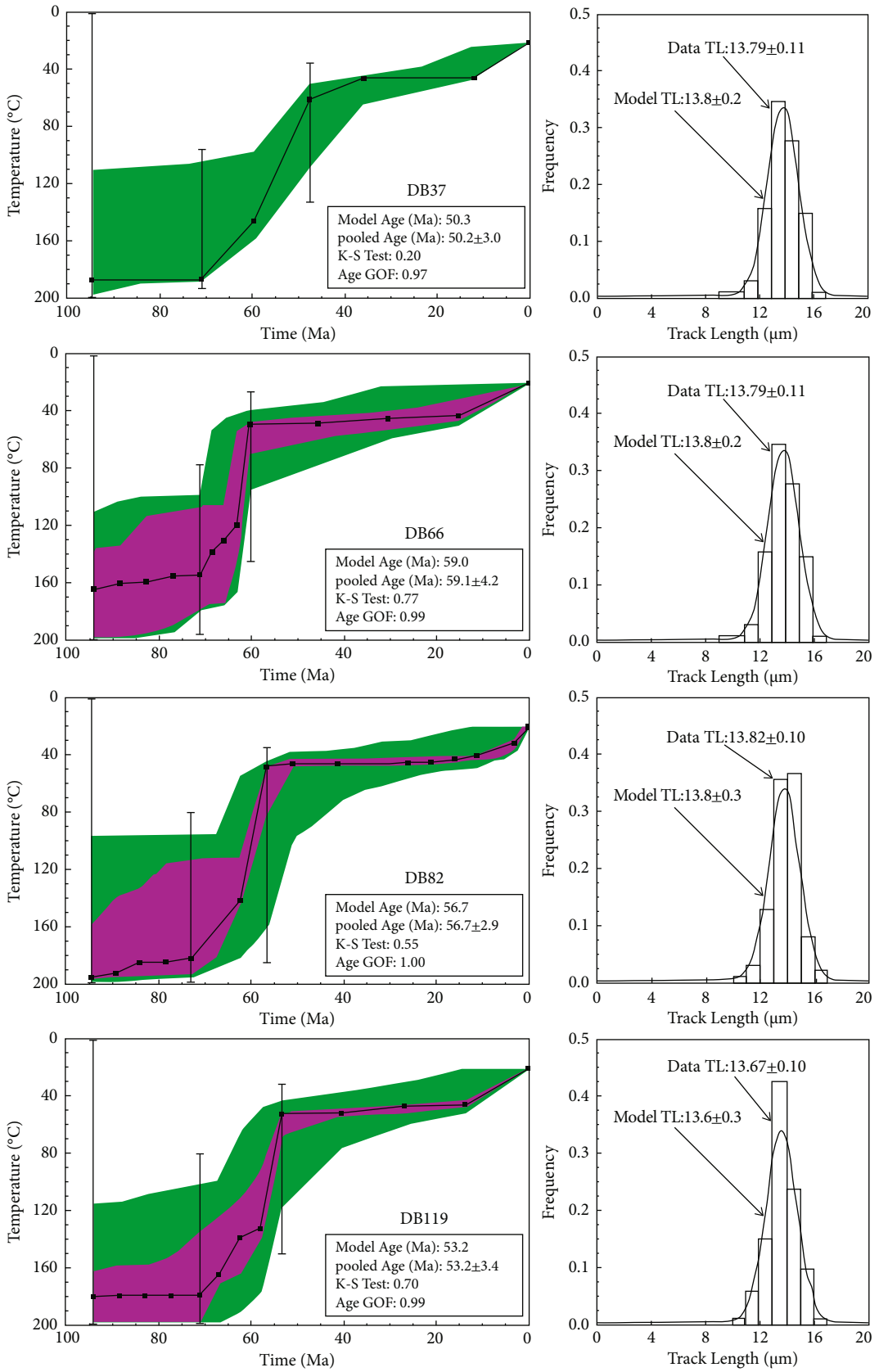

Figure 6: Exhumation history simulation diagram of AFTs and histogram of AFT length distribution in the ore-hosting rock body. The solid line marks the best-fit time-temperature path from which the simulated data were derived. Green regions mark envelopes of statistically acceptable fits. Magenta regions indicate envelopes for statistically good fits. I-bars mark user-entered time-temperature constraints.

Table 3: Sample locations and exhumation depth of the Duobaoshan rock body.

Sample number	Longitude E	Latitude N	Exhumation depth (km)	Exhumation rate (mm/yr)	Lithology
DB01	125°46′50″	50°14′37″	3.11	0.27	Wallrock
DB82	125°47′02″	50°14′36″	3.86	0.24	Ore body
DB37	125°46′51″	50°14′54″	3.77	0.16	Ore body
DB66	125°47′08″	50°14′49″	2.99	0.28	Ore body
DB119	125°47′20″	50°14′28″	3.62	0.21	Ore body
DB120	125°47′26″	50°14′53″	2.33	0.22	Wallrock
DB07	125°46′59″	50°15′08″	3.9	0.11	Diorite vein
DB98	125°47′10″	50°14′41″	3.92	0.11	Diorite vein
DB14	125°47′19″	50°14′51″	2.94	0.51	Trondhjemite
DB18	125°47′16″	50°14′57″	2.29	0.19	Trondhjemite
DB99	125°47′14″	50°14′51″	2.42	0.09	Trondhjemite
DB118	125°47′24″	50°14′32″	2.71	0.08	Granite porphyry

Note: The exhumation dates of DB07 to DB118 from Leng [50] .

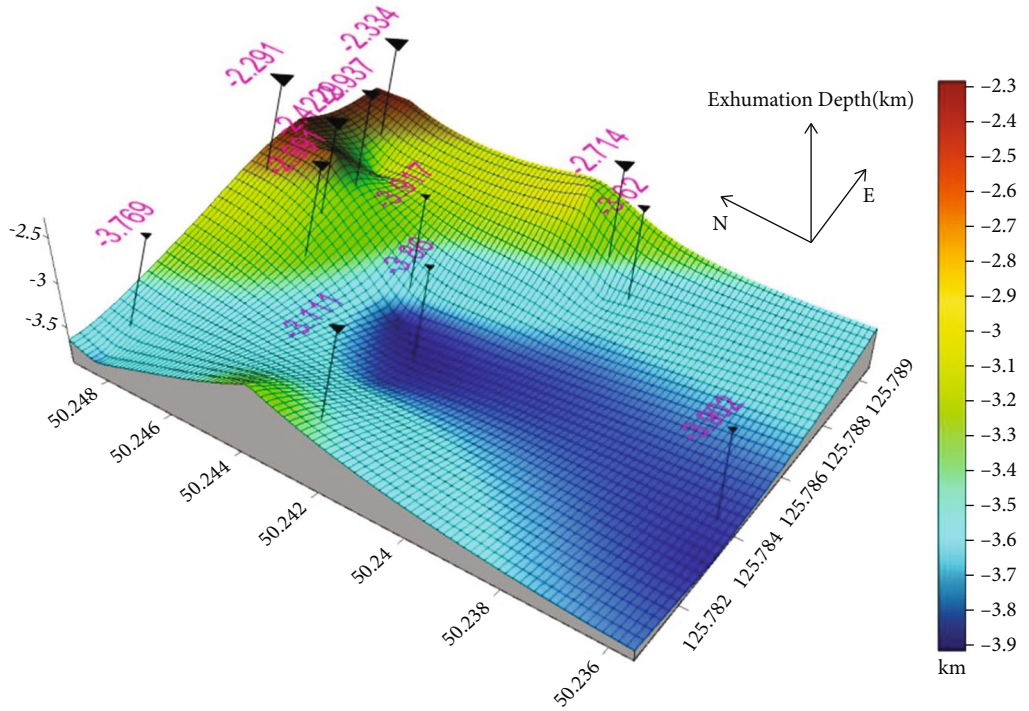

Figure 7: Three-dimensional model of exhumation after the formation of the Duobaoshan copper deposit.

the rock body starting from the Late Cretaceous, but the rapid cooling stage of the "surrounding rock body" and the "ore body" was not synchronous. For the surrounding rock body: A. for a period of time before 82 Ma, the rock body was basically in a stable stage; B. around 82–72 Ma, a rapid cooling stage; C. after 71 Ma, a slow cooling stage. For the NW-trending ore body: A. for a period of time before 71.8 Ma, the ore body was basically in a stable stage; B. around 71.8–50.2 Ma, a rapid cooling stage; C. after 50.2 Ma, a slow cooling stage. Therefore, the surrounding rock body began to undergo rapid cooling earlier than the NW-trending ore body, but the two periods of cooling were basically continuous and partial annealing occurred only once. This differential exhumation and cooling event enabled the Duobaoshan Paleozoic porphyry copper deposit to be favorably preserved. At the same time, it has certain

practical significance for guiding the prospecting of ancient porphyry deposits in the world. Combination the evidence of the geotectonic evolution of the mining area and of the exhumation and cooling evolution process of the ore-bearing rock body, the mining area underwent both compressional tectonism and extensional tectonism in the Yanshanian. During this period, there was obvious rapid exhumation and cooling, and the rock body was then basically stable until the Eocene period. This coincided with an cooling and exhumation event in the Late Cretaceous period in eastern China. In the Campanian, the Okhotomorsk Block collided with the Siberian margin in northeast Asia. At about 77 Ma, new oceanic subduction occurred to the south of the block, ending its long-distance northward motion [49]. Correspondingly, the contact between the Sifangtai and Nenjiang formations is a regional unconformity of the Late Cretaceous in the Songliao Basin, northeast China.

Based on the AFT thermal tectonic chronology analysis results combined with the sampling location and exhumation depth data of the Duobaoshan rock body (Table 3), the three-dimensional model of uplift and exhumation after the formation of the Duobaoshan Cu (Mo) deposit was established, as shown in Figure 7. Because of the impact of differential uplift tectonic activity in the mining area, the rock body exhumation depth is greater in the middle of the mining area, resulting in the formation of an open-pit deposit in the ore body.

6.3. Tectonic setting of the Duobaoshan porphyry copper deposits. The formation of the early Paleozoic Duobaoshan porphyry Cu (Mo) deposit is related not only to the integration of the Xing'an and Erguna blocks, but also to uplift after the collision between the Xing'an and Songnen blocks [51]. The Erguna block became stable in the early Paleozoic [22, 23], and the Xing'an block accreted to the Erguna block along the Tayuan–Xiguitu fault in the middle of the early Paleozoic, whereas the Songnen block was collaged with the above combined blocks along the Hegenshan–Nenjiang fault in the late Paleozoic. In the early Mesozoic, the Jiamusi block merged with the above combined blocks along the Mudanjiang fault and the Xingmeng–Mongolia orogenic belt [7], and merged into the coastal Pacific continental margin active zone to enter an intraplate deformation stage. In the early Mesozoic (~227 Ma) [52], the Duobaoshan copper mining area was affected by the subduction of the Paleo-Pacific plate, the early fault was activated, and there were volcanic eruptions and homologous granite intrusions, forming the Mesozoic intraplate volcanic rock belt of the Great Hinggan Mountains [10]. In the Jurassic–Cretaceous, fault deformation and magmatic activity were intense. In the Middle Jurassic, the area may have been affected by the Nenjiang deep fault activity, and the Early Yanshanian granodiorite and quartz monzodiorite intruded along the NNE- and NNW-trending faults on the east side of the mining area. During the Late Jurassic to Middle and Late Early Cretaceous, NNE- or NE-trending fault structures were produced in the mining area, possibly because of interaction between the Kula-Pacific plate and the East Asian continent and the influence of mantle uplift. After the Late Cretaceous, compressional uplift was the main tectonic movement in this area, leading to differential uplift and cooling events in the Duobaoshan mining area [19, 53].

7. Conclusions

(1) The AFT age distribution of granite samples from the Duobaoshan copper deposit varied from 50.2 ± 3.0 to 76.0 ± 3.8 Ma. These dates recorded the exhumation and cooling events of the Duobaoshan area in the Late Cretaceous-Eocene period and demonstrate the occurrence of Late Yanshanian tectonic movement in the Duobaoshan region

(2) The exhumation history simulation results indicate that the Duobaoshan granite body went through a rapid exhumation and cooling event during the Late Cretaceous to Eocene period (82–50.2 Ma). The average cooling rate of the surrounding rock body was about 0.25 mm/a. The average cooling rate of the orebody was about 0.22 mm/a. Since the Eocene period (50.2 Ma), the crust of the Duobaoshan region has been basically stable

(3) The AFT age characteristics and spatial distribution of ore bodies indicate that starting in the Late Cretaceous period, the Duobaoshan granite was exhumated by compression, and the NW-trending ore-hosting rock body was exhumated later than the surrounding rock body, which caused differential exhumation between the ore body and the surrounding rock body, providing favorable geological conditions for the preservation of the ore body

Data Availability

The data used to support the findings of this study are included within the article and are available from the corresponding author upon request.

Conflicts of Interest

The authors declare that there is no conflict of interest regarding the publication of this paper.

Funding

This research was jointly supported by the National Natural Science Foundation of China (Nos. 41730426, 41272106 and 41233011).

Acknowledgments

The authors are thankful to Researchers Jishun Ren, Xinhua Zhou and Zhigang Xu for improving the text. We thank Sara J. Mason, MSc, from Liwen Bianji, Edanz Editing China, for editing the English text of a draft of this manuscript. We appreciate the editor and the anonymous reviewers for their constructive comments on this manuscript.

References

[1] D. R. Cooke, P. Holling, and J. L. Walshe, "Giant porphyry Deposits: characteristics, distribution, and tectonic controls," *Econonmic Geology*, vol. 100, no. 5, pp. 801–818, 2005.

[2] X. Sun, P. Hollings, and Y. J. Lu, "Geology and origin of the Zhunuo porphyry copper deposit Gangdese belt, southern Tibet," *Mineralium Deposita*, vol. 56, no. 3, pp. 457–480, 2021.

[3] E. Seedorff, J. H. Dilles, J. M. Proffett, M. T. Einaudi, and M. Barton, "Porphyry Deposits Characteristics and origin of hypogene Features," *Econonmic Geology*, vol. 100, pp. 251–298, 2005.

[4] D. H. Zhang, J. H. Xu, X. Q. Yu et al., "The diagenetic and metallogenic depth: main constriants and the estimation methods," *Geological Bulletin of China*, vol. 30, no. 1, pp. 112–125, 2011.

[5] J. Liu, G. Wu, Y. Li, M. T. Zhu, and W. Zhong, "Re-Os sulfide (chalcopyrite, pyrite and molybdenite) systematics and fluid inclusion study of the Duobaoshan porphyry cu (Mo) deposit, Heilongjiang Province, China," *Journal of Asian Earth Sciences*, vol. 49, pp. 300–312, 2012.

[6] G. Cui, J. Y. Wang, J. X. Zhang, and G. Cui, "U-Pb SHRIMP dating of zircons from Duobaoshan granodiorite in Heilongjiang and its geological significance," *Global Geology*, vol. 27, no. 4, pp. 387–394, 2008.

[7] W. C. Ge, F. Y. Wu, C. Y. Zhou, and J. H. Zhang, "Porphyry cu-Mo deposits in the eastern Xing'an-Mongolian Orogenic Belt: mineralization ages and their geodynamic implications," *Chinese Science Bulletin*, vol. 52, no. 24, pp. 3416–3427, 2007.

[8] Q. Du and M. X. Chen, "The genetic model of Duobaoshan porphyry copper deposits," *Mineral Deposit*, vol. 2, no. 2, pp. 42–48, 1983.

[9] Y. Y. Zhao, Z. H. Ma, and B. Z. Feng, "Geochemical exploration model of Duobaoshan copper deposit Heilongjiang," *Journal of Guilin Institute of technology*, vol. 17, no. 1, pp. 48–54, 1997.

[10] G. Wu, Y. H. Chen, F. Y. Sun, J. Liu, G. R. Wang, and B. Xu, "Geochronology, geochemistry, and Sr-Nd-Hf isotopes of the early Paleozoic igneous rocks in the Duobaoshan area, NE China, and their geological significance," *Journal of Asian Earth Sciences*, vol. 97, no. 1, pp. 229–250, 2015.

[11] H. Zeng, Y. Y. Zhao, J. J. Fu, and Y. Li, "Features of sulfide and Plumbum isotopes of the copper deposits in Duobaoshan deposit cluster in Heilongjiang Province, China," *Acta Geology Sinica*, vol. 88, no. s2, pp. 643-644, 2014.

[12] Y. Li, X. Y. Hou, B. Yang, Y. Y. Zhao, and L. Chen, "Indo-Chinese magmatic activity in the Duobaoshan District of Heilongjiang Province and its geological significance," *Acta Geologica Sinca*, vol. 91, no. 6, pp. 2058–2077, 2017.

[13] Q. D. Zeng, J. M. Liu, S. X. Chu et al., "Re-Os and U-Pb geochronology of the Duobaoshan porphyry cu-Mo-(au) deposit, Northeast China, and its geological significance," *Journal of Asian Earth Sciences*, vol. 79, pp. 895–909, 2014.

[14] H. Wei, J. H. Xu, Q. D. Zeng, Y. H. Wang, J. M. Liu, and S. X. Chu, "Fluid evolution of alteration and mineralization at the Duobaoshan porphyry cu (Mo) deposit, Heilongjiang Province," *Acta Petrologica Sinica*, vol. 27, no. 5, pp. 1361–1374, 2011.

[15] Y. Y. Zhao, J. P. Wang, G. J. Zhao, and Y. B. Cui, "Metallogenic regularities and prospecting direction of Duobaoshan ore field, Heilongjiang Province, China," *Journal of Earth Science-Jilin University*, vol. 41, no. 6, pp. 1676–1688, 2011.

[16] Z. H. Zhao, W. Z. Zheng, H. Qu et al., "Cu-au mineralization and metallogenic regularity of Duobaoshan area, Heilongjiang Province," *Mineral Deposit*, vol. 31, no. 3, pp. 601–614, 2012.

[17] J. Liu, Y. Li, Z. H. Zhou, and H. G. Ouyang, "The Ordovician igneous rocks with high Sr/Y at the Tongshan porphyry copper deposit, satellite of the Duobaoshan deposit, and their metallogenic role," *Ore Geology Reviews*, vol. 86, pp. 600–614, 2017.

[18] Q. Du, Y. M. Zhao, B. G. Lu et al., *The Duobaoshan porphyry copper deposit*, Geological Publishing House, Beijing, 1988.

[19] Y. M. Zhao and D. Q. Zhang, *Metallogeny and Prospective Evalution of Copper–Polymetallic Deposits in the Great Hinggan Range and Its Adjacent Regions*, Seismological Press, Beijing, 1997.

[20] Z. X. Han, Y. Q. Xu, and Q. D. Zheng, *Metallogenetic Series and Evolution of Significant Metal and Nonmetal Mineral Resources in Heilongjiang Province*, Heilongjiang People's Publishing House, Harbin, 2004.

[21] G. Wu, J. Liu, W. Zhong, M. T. Zhu, M. Mei, and Q. Wan, "Fluid inclusion study of the Tongshan porphyry copper deposit, Heilongjiang province, China," *Acta Petrologica Sinica*, vol. 25, no. 11, pp. 303–314, 2009.

[22] W. C. Ge, F. Y. Wu, C. Y. Zhou, and A. A. A. Rahman, "Geochronology and Metallogenic regularity of the Tahe granite in the northern Daxingan Mountains and its restriction on the structure of Ergonga block," *Chinese Science Bulletin*, vol. 50, no. 12, pp. 1239–1247, 2005.

[23] G. Wu, F. Y. Sun, C. S. Zhao, Z. T. Li, Q. B. Pang, and G. Y. Li, "Discovery of early Paleozoic post-collisional granite in the northern margin of Erguna and its geological significance," *Chinese Science Bulletin*, vol. 50, no. 20, pp. 2278–2288, 2005.

[24] X. C. Wang, J. Y. Liu, Y. Z. Zhao, L. S. Wan, and C. S. Bai, "Prospecting 'Kalamazoo' type of copper deposit in China," *Heilongjiang Geology*, vol. 9, no. 3, pp. 1–9, 1998.

[25] Y. J. Hao, Y. S. Ren, M. X. Duan et al., "Metallogenic events and tectonic setting of the Duobaoshan ore field in Heilongjiang Province, NE China," *Journal of Asian Earth Sciences*, vol. 97, pp. 442–458, 2015.

[26] Y. J. Chen, H. Y. Chen, K. Zaw, F. Pirajno, and Z. J. Zhang, "Geodynamic settings and tectonic model of skarn gold deposits in China: an overview," *Ore Geology Reviews*, vol. 31, no. 1–4, pp. 139–169, 2007.

[27] Z. T. Li, X. J. Wang, H. B. Wang, and G. Wu, "Geology of the Sankuanggou goldbearing iron–copper deposit in Nenjiang County, Heilongjiang Province," *Geology and Resources*, vol. 17, no. 3, pp. 170–174, 2008.

[28] R. A. Ketcham and M. T. Tamer, "Confined fission track revelation in apatite: how it works and why it matters," *Geochronology*, vol. 3, 2021.

[29] R. A. Donelick and D. S. Miller, "Enhanced TINT fission track densities in low spontaneous track density apatites using 252Cf-derived fission fragment tracks: a model and experimental observations," *International Journal of Radiation Applications*, vol. 18, no. 3, pp. 301–307, 1991.

[30] A. J. Hurford and P. F. Green, "A users' guide to fission track dating calibration," *Earth and Planetary Science Letters*, vol. 59, no. 2, pp. 343–354, 1982.

[31] R. A. Ketcham, A. Carter, R. A. Donelick, J. Barbarand, and A. J. Hurford, "Improved modeling of fission-track annealing

in apatite," *American Mineralogist*, vol. 92, no. 5-6, pp. 799–810, 2007.

[32] R. F. Galbraith and G. M. Laslett, "Statistical models for mixed fission track ages," *Nuclear Tracks and Radiation Measurements*, vol. 21, no. 4, pp. 459–470, 1993.

[33] E. R. Sobel, O. Michael, B. Douglas, and M. Alexer, "Exhumation of basement-cored uplifts: example of the Kyrgyz range quantified with apatite fission track thermochronolgy," *Tectonics*, vol. 25, no. 2, pp. 1–17, 2006.

[34] R. F. Galbraith, "On statistical models for fission track counts," *Mathematical Geology*, vol. 13, no. 6, pp. 471–478, 1981.

[35] J. Barbarand, A. Carter, I. Wood, and T. Hurford, "Compositional and structural control of fission-track annealing in apatite," *Chemical Geology*, vol. 198, no. 1-2, pp. 107–137, 2003.

[36] W. D. Carlson, R. A. Donelick, and R. A. Ketcham, "Variability of apatite fission-track annealing kinetics: I. experimental results," *American Mineralogist*, vol. 84, no. 9, pp. 1213–1223, 1999.

[37] R. A. Ketcham, "Forward and inverse modeling of low-temperature thermochronometry data," *Reviews in Mineralogy Geochemistry*, vol. 58, no. 1, pp. 275–314, 2005.

[38] A. J. W. Gleadow, L. R. Duddy, P. F. Green, and K. A. Hegarty, "Fission track lengths in the apatite annealing zone and the interpretation of mixed ages," *Earth and Planetary Science Letters*, vol. 78, no. 2–3, pp. 245–254, 1986.

[39] P. F. Green, I. R. Duddy, G. M. Laslett, K. A. Hegarty, A. J. W. Gleadow, and J. F. Lovering, "Thermal annealing of fission tracks in apatite 4. Quantitative modelling techniques and extension to geological timescales," *Chemical Geology Isotope Geoscience*, vol. 79, no. 2, pp. 155–182, 1989.

[40] J. H. Liu, P. Z. Zhang, D. W. Zheng, J. L. Wan, and W. T. Wang, "The cooling history of Cenozoic exhumation and uplift of the Taibai mountains, Qinling, Cnina: evidence from apatite fission track (AFT) analysis," *Chinese Journal of Geophysics*, vol. 53, no. 10, pp. 2405–2414, 2010.

[41] A. J. W. Gleadow, I. R. Duddy, P. F. Green, and J. F. Lovering, "Confined fission track lengths in apatite: a diagnostic tool for thermal history analysis," *Contributions to Mineralogy and Petrology*, vol. 94, no. 4, pp. 405–415, 1986.

[42] T. S. Kang and S. C. Wang, *Fission track method of geological thermal history studies*, Science Press, Beijing, 1991.

[43] Y. Sun, Z. L. Chen, B. L. Chen et al., "Cenozoic uplift and denudation of the EW-trending range of northern Altun Mountains: evidence from apatite fission track data," *Acta Geosciencetica Sinica*, vol. 35, no. 1, pp. 67–75, 2014.

[44] R. A. Ketcham, R. A. Donelick, and W. D. Carlson, "Variability of apatite fission track annealing kinetics III: extrapolation to geological time scales," *American Mineralogist*, vol. 84, no. 9, pp. 1235–1255, 1999.

[45] P. V. D. Beek, X. Robert, J. L. Mugnier, M. Bernet, P. Huyghe, and E. Labrin, "Late Miocene-recent exhumation of the central Himalaya and recycling in the foreland basin assessed by apatite fission-track thermochronology of Siwalik sediments, Nepal," *Basin Research*, vol. 18, no. 4, pp. 413–434, 2006.

[46] G. M. Laslett, P. F. Green, I. R. Duddy, and A. J. W. Gleadow, "Thermal annealing of fission tracks in apatite 2. A quantitative analysis," *Chemical Geology: Isotope Geoscience Section*, vol. 65, no. 1, pp. 1–13, 1987.

[47] K. Gallagher, "Evolving temperature histories from apatite fission-track data," *Earth and Planetary Science Letters*, vol. 136, no. 3-4, pp. 421–435, 1995.

[48] X. M. Li, X. Y. Yang, B. Xia et al., "Exhumation of the Dahinggan Mountains, NE China from the late Mesozoic to the Cenozoic: new evidence from fission-track thermochronology," *Journal of Asian Earth Sciences*, vol. 42, no. 1-2, pp. 123–133, 2011.

[49] Y. T. Yang, "An unrecognized major collision of the Okhotomorsk Block with East Asia during the Late Cretaceous, constraints on the plate reorganization of the Northwest Pacific," *Earth-Science Reviews*, vol. 126, pp. 96–115, 2013.

[50] Y. X. Leng, *Emplacement depth of the granitic complex, post-ore change and preservation of the Duobaoshan Prophyry Cu(Mo) Deposit, Heilongjiang Province, China, [M.S. thesis]*, China University of Geosciences, Beijing, 2016.

[51] B. C. Yin and Q. C. Ran, "The tectonic environment of metallogenesis of Duobaoshan superlarge copper deposit," *Acta Mineralogica Sinica*, vol. 17, no. 2, pp. 220–224, 1997.

[52] K. Y. Zhu, Z. X. Li, X. S. Xu, and S. A. Wilde, "Late Triassic melting of a thickened crust in southeastern China: evidence for flat-slab subduction of the paleo-Pacific plate," *Journal of Asian Earth Sciences*, vol. 74, pp. 265–279, 2013.

[53] Z. L. Ren, J. P. Cui, Z. Shi, F. F. Bai, and H. Li, "The late Paleozoic tectonic evolution and later transformation in Northeast China," *Oil & Gas Geology*, vol. 31, no. 6, pp. 0734–0742, 2010.